Dossier

This paper is a part of the hereunder thematic dossier published in OGST Journal, Vol. 70, No. 6, pp. 909-1132 and available online here

Cet article fait partie du dossier thématique ci-dessous publié dans la revue OGST, Vol. 70, n°6, pp. 909-1132 et téléchargeable ici

Oil & Gas Science and Technology – Rev. IFP Energies nouvelles, Vol. 70 (2015), No. 6, pp. 909-1132

IFP Energies nouvelles

Oil & Gas Science and Technology – Rev. IFP Energies nouvelles, Vol. 70 (2015), No. 6, pp. 951-965

DOI: 10.2516/ogst/2012021

Computer Modeling of the Displacement Behavior of Carbon Dioxide in Undersaturated Oil Reservoirs

Binshan Ju[1]*, Yu-Shu Wu[2], Jishun Qin[3]

1 School of Energy Resources, China University of Geosciences, Xueyuan Road No.29, Beijing, 100083 - P.R. China
2 Colorado School of Mines, 80401, Colorado - USA
3 PetroChina Research Institute of Petroleum Exploration and Development, Xueyuan Road No.20, Beijing, 100083 - P.R. China
e-mail: jubs2936@163.com - ywu@mines.edu - qinjs@petrochina.com.cn

* Corresponding author

Résumé — Modélisation par ordinateur du comportement de déplacement du dioxyde de carbone dans des réservoirs d'huile non saturés — L'injection de CO_2 dans des réservoirs d'huile est réalisée non seulement pour améliorer la récupération d'huile mais aussi pour stocker le CO_2 émis par la combustion de combustibles fossiles. L'objectif de ce travail est de développer un simulateur numérique pour prédire quantitativement les écoulements de CO_2 supercritique pour la récupération assistée d'hydrocarbures (EOR ; *Enhanced Oil Recovery*). Un modèle mathématique d'écoulement compositionnel non isotherme est développé. Le diagramme de transition de phase est conçu à partir de la Pression de Miscibilite Minimum (PMM) et de la solubilité maximum de CO_2 dans l'huile. La convection et la diffusion des mélanges de CO_2 dans les fluides à phases multiples se trouvant dans les réservoirs, le transfert de masse entre le CO_2 et le brut ainsi que la séparation de phase sont pris en considération. Les équations directrices sont discrétisées en appliquant une technique de différences finies complètement implicite. La technique itérative de Newton-Raphson a été utilisée pour résoudre les systèmes d'équations non linéaires et un simulateur a été développé. Les performances des écoulements de CO_2 non miscible et miscible au sein des réservoirs d'huile sont prédites par le nouveau simulateur. La distribution de pression et de température, les saturations de phase, la fraction molaire de chaque composant dans chaque phase, les dommages à la formation provoqués par la précipitation d'asphaltène et la récupération améliorée d'huile sont prédits par le simulateur. Les données expérimentales valident le simulateur développé par comparaison avec les résultats de simulation. Les applications du simulateur en matière d'écoulement de CO_2 dans les réservoirs d'huile indiquent que le simulateur est robuste pour la prédiction des performances des écoulements de CO_2.

Abstract — Computer Modeling of the Displacement Behavior of Carbon Dioxide in Undersaturated Oil Reservoirs — *The injection of CO_2 into oil reservoirs is performed not only to improve oil recovery but also to store CO_2 captured from fuel combustion. The objective of this work is to develop a numerical simulator to predict quantitatively supercritical CO_2 flooding behaviors for Enhanced Oil Recovery (EOR). A non-isothermal compositional flow mathematical model is developed. The phase transition diagram is designed according to the Minimum Miscibility Pressure (MMP) and CO_2 maximum solubility in oil phase. The convection and diffusion of CO_2 mixtures in multiphase fluids in reservoirs, mass transfer between CO_2 and crude and phase partitioning are considered. The governing equations are discretized by applying a fully implicit finite difference technique. Newton-Raphson iterative technique was used to solve the nonlinear equation systems and a simulator was developed. The performances of CO_2 immiscible and miscible flooding in oil reservoirs are predicted by the new*

simulator. The distribution of pressure and temperature, phase saturations, mole fraction of each component in each phase, formation damage caused by asphaltene precipitation and the improved oil recovery are predicted by the simulator. Experimental data validate the developed simulator by comparison with simulation results. The applications of the simulator in prediction of CO_2 flooding in oil reservoirs indicate that the simulator is robust for predicting CO_2 flooding performance.

NOMENCLATURE

a	"Attraction" parameter in state equation
A^k	Accumulation term of component k per unit bulk volume (kg/m^3)
A'	Parameter in the correlation for calculating viscosity
d^k_β	Molecular diffusion coefficient of component k within fluid β (m^2/s)
b	"Repulsion" parameter in state equation
B'	Parameter in the correlation for calculating viscosity
c	Parameter in state equation
C^k_s	Concentration of component k in gas phase (kg/m^3)
C_{perm}	Permeability change
C'	Parameter in the correlation for calculating viscosity
$\underline{D}^k_\beta$	Hydrodynamic dispersion tensor accounting for both molecular diffusion and mechanical dispersion for component k in phase β (m^2/s)
D'	Parameter in the correlation for calculating viscosity
f	Flow efficiency factor
f_{RF}	Mole fraction of components, C_2-C_4
F^k	"Flow" term of mass or diffusive and dispersive mass transport per unit bulk volume (kg/(s.m^3))
g	Gravitational constant (m/s^2)
h_β	Specific enthalpy of fluid phase β (J/kg)
h^k_β	Specific enthalpy of component k in fluid β (J/kg)
k	Index for the components
k'	Absolute permeability (m^2)
k'_0	Initial absolute permeability (m^2)
$k'_{r\beta}$	Relative permeability to phase β
K_{CT}	Overall thermal conductivity (W/(m.°C))
$K^k_{\alpha:\beta}$	Equilibrium partitioning coefficient of component k between phases α and β
MMP	Minimum Miscibility Pressure (Pa)
$M_{C_7^+}$	Molar weight of C_7^+ (g)
N_c	Total number of mass components
R^k_s	Adsorption term of component k on rock solids
P_C	Capillary pressure (Pa)
P_β	Pressure of phase β (Pa)
q^k	External source/sink term for mass component k (kg/(s·m^3))
q^T	External source/sink terms for energy (W/(s.m^3))
R	Universal gas constant (8.3145 J/mol.K)
R^k_s	Adsorption rate of component k on rock solids (1/s)
S_β	Saturation of phase β
t	Time (s)
T	Temperature in EOS (K)
T_C	Critical temperature (°C)
T_{RC}	Reservoir temperature (°C)
U_s	Internal energies rock solids (J/kg)
U_β	Internal energies of fluid β (J/kg)
$\mathbf{v}_o$	Flow velocity of oil phase (m/s)
$\mathbf{v}_\beta$	Vector of volumetric flow rate for phase β (m/s)
V	Volume (m^3)
x	Coordinate at X direction (m)
X^k_β	Mole fraction of component k in phase β
y	Coordinate at Y direction (m)
z	Coordinate at Z direction (m)

Greek symbols

α^k_d	Capture rate constant of component k (m^{-1})
α^β_L	Longitudinal dispersivities (m)
α^β_T	Transverse dispersivities (m)
β_m	Parameter in state equation
δ^k	Volume of component k deposited on the pore surfaces per unit bulk volume
δ_{ij}	Kronecker delta function
ϕ	Porosity of a porous medium
ϕ'	Instaneous porosity considering asphaltene precipitation
λ_f	Constant for fluid seepage allowed by the plugged pores
μ_β	Viscosity of fluid phase β (Pa.s)
ρ_s	Density of rock solids (kg/m^3)
ρ_β	Density of phase β (kg/m^3)
τ	Tortuosity of a porous medium
ω_i	Acentric factor of the hydrocarbon component i

Subscripts

0	Initial time
g	Gas
m	Mixture
o	Oil
w	Water
β	An index for fluid phase

INTRODUCTION

During the period since 1750, CO_2 concentration in the atmosphere has increased from 280 ppm to 368 ppm in 2000 and 388 ppm in 2010 (Rackley, 2010). Annual CO_2 emission in the 11 southeastern states (Alabama, Arkansas, Florida, Georgia, Louisiana, Mississippi, North Carolina, South Carolina, Tennessee, Virginia and east Texas), of USA is up to about 1045 million metric tons (Petrusak *et al*., 2009). Chinese existing and planned projects (nearly 400) for making ammonia, methanol and other fuels from coal will emit some 270 million tonnes of CO_2 per annum (Zheng *et al*., 2010). The CO_2 concentration in the atmosphere is increasing at the rate of 2 ppm yearly. Increase in atmospheric emission of CO_2 with the attendant global warming and environmental degradation are driven by global energy demand (Lal, 2008).

Depleted or mature oil fields may provide feasible sites for storing CO_2 in porous and permeable reservoirs (Petrusak *et al*., 2009; Shtepani, 2006). CO_2 is injected into an oil reservoir to reduce oil viscosity and interfacial tension, and cause oil swelling, which improves oil recovery (Jaramillo *et al*., 2009). In most oil reservoirs, CO_2 is a supercritical fluid as reservoir conditions are above its critical temperature (31.4°C) and pressure (7.4 MPa). Supercritical CO_2 is a favorable flooding agent for EOR. Many oil fields in main oil production countries offer good opportunities for CO_2 injection in oil formations for EOR purposes. The history of CO_2 flooding for EOR purpose in oil fields and successful projects verifies that it can improve oil recovery to a larger extent. However, one adverse factor of CO_2 flooding for EOR is the problem induced by asphaltene precipitation and deposition. It may not only lead to the formation damages by reducing porosity and permeability (Shedid and Zekri, 2006) but also have some adverse influences on production facilities such as tubing and pumps (Thawer *et al*., 1990; Rashid and Sultan, 2003).

During CO_2 flow in oil reservoirs, the main physical and chemical interactions among the water, crude oil and rocks include:

- the immiscible and miscible displacement of oil, water and CO_2;
- convection and diffusion;
- phase change and behavior of *in-situ* fluids on flow and mass transfer;
- asphaltene precipitation and its effects on porosity and permeability.

Currently, several simulators have been developed for simulating the CO_2 flow in saline aquifers and coal beds. Among these simulators, TOUGH2-ECO2N (Pruess, 2005), TOUGH2-ECO2M (Pruess, 2011), MUFTE (Bielinski, 2007), GEM (Nghiem *et al*., 2004), NUFT (Nitao, 1998), FLOTRAN (Lichtner, 2003), STOMP (White, 2003) can be used to simulate the process of CO_2 injection into aquifers. TOUGH2-ECO2N (one member of TOUGH2 family) provides a flexible grid treatment and robust numerical solver to solve the multiphase flow equations in porous media. PSU-COALCOMP (Sams *et al*., 2002) and SIMED (Pinczewski and Stevenson, 2007) were reported to simulate the flow of CO_2 in coal beds. However, the above simulators provide the approaches for simulating CO_2 sequestration in aquifer formation or coal beds. TOUGH2-TMGAS (Battistelli and Marcolini, 2009) can be used to model the two-phase equilibrium between NaCl brine and non-aqueous phase mixtures made up by both organic and inorganic components. The main limitation of the approach is that only two-phase conditions are allowed. Especially, the physical and chemical mechanisms of CO_2 flooding for EOR differ from the CO_2 sequestration in aquifer and coal beds. More recently, ECLIPSE 300 and CMG-GEM modules has been developed for predicting the CO_2 flooding performances for EOR. Peng-Robinson's (PR) and Soave-Redlich-Kwong's (SRK) equations are selected to predict phase equilibrium and properties in the above simulators. However, high CO_2 concentration dissolved in crude oil at reservoir conditions will lead to the severe inaccurate prediction of CO_2-oil mixture properties such as densities and compressibility factors.

The authors developed a non-isothermal compositional mathematical model as well as a reservoir simulator for quantitative description of processes in CO_2 flooding and subsurface storage in reservoirs. The formation damage caused by asphaltene precipitation and its effect on the performances of oil production are also considered in the model. The MMP and CO_2 solubility in crude oil were chosen as the criterions for phase transfer. Four simulation examples were designed to demonstrate the various functions of the simulator developed in this work. It is found that the predicted recovery flooded by CO_2 injection at a miscible condition has a good match with the experimental data.

1 MATHEMATICAL MODEL AND GOVERNING EQUATIONS

1.1 Assumptions and Considerations

Physical and chemical processes of CO_2 flow and transport are simulated by using a conceptual model of multiphase fluid flow and multi-component transport in porous media. The CO_2-EOR mathematical model is based on the following assumptions and considerations:

- heat transfer in porous media is considered;
- flow and transport mechanisms include multiphase Darcy's flow and multi-component diffusion, subject to adsorption and precipitation;
- incorporation of a number of mass components: CO_2, H_2O, oil with some pseudo-oil components;

– description of CO_2 adsorption on pore walls of reservoir formations;
– dissolution of CO_2 in oil;
– phase change and behavior of multiphase and multi-component systems of CO_2, oil and water on flow, displacement in reservoirs;
– porosity and permeability changes induced by asphaltene deposition on pore walls are considered.

1.2 Phase Behavior and Fluid Types

The base case scenarios of fluid phases in the model are:
– two phases of water and crude oil (pressure is lower than MMP without free CO_2 phase);
– three phases of water, gas and oil under reservoir pressure below MMP;
– two phases of water and CO_2-oil mixture above MMP.

1.3 Phase Transfer and Condition

According to thermodynamic conditions and relative abundance of the different components, the fluids may exist in three scenarios, as shown in Figure 1. Arrows denote routes for appearance or disappearance of phases that are checked after the updates of primary variables. There are two key parameters (MMP and CO_2 equilibrium solubility in oil) determining phase switch in Figure 1.

Before CO_2 injection into undersaturated reservoirs, only oil and water phases coexist (see scenario 1). If the reservoir pressure is less than MMP or equal to MMP, scenario (1) will switch to scenario (2) if the CO_2 solubility exceeds its saturation state. If the pressure becomes larger than MMP, no free CO_2 releases and CO_2-hydrocarbons will arrive at miscible state. In this case, scenario (1) will switch to scenario (3).

For scenario (2), when the pressure becomes lower than MMP or equal to MMP and if free gas disappears, then scenario (2) will switch to scenario (1). If the pressure exceeds MMP, the gas dissolves into oil. In this case, scenario (2) will switch to scenario (3).

For scenario (3), when the pressure becomes lower than MMP and if the CO_2 solubility does not reach its saturation state, then scenario (3) will switch to scenario (1). If the pressure becomes less than MMP, the free gas releases from oil. In this case, scenario (3) will switch to scenario (2).

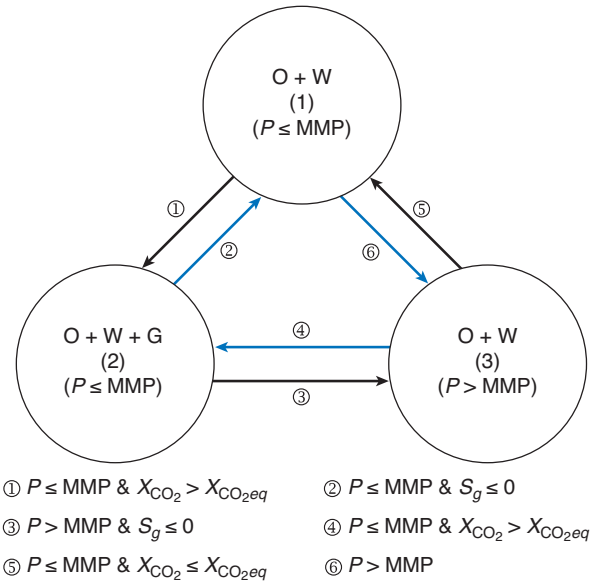

O: Oil phase or Oil-CO_2 mixture phase; W: Water phase; G: Gas phase; P: Pressure; MMP: Minimum miscibility pressure; Sg: Gas (CO_2) saturation. X_{CO_2}: CO_2 mole fraction dissolved in oil phase; X_{CO_2eq}: Maximum CO_2 mole fraction dissolved in oil phase when equilibrium reaches at given pressure and temperature.

Figure 1

Phase scenarios and transfer path diagram (Note: gas phase is a special component mixture, including CO_2, methane, ethane and other light hydrocarbons. At reservoir conditions, the phase may be at a supercritical state. Therefore, gas phase specified in this work might not be a real gas state condition).

1.3.1 MMP Calculation

A feasible approach for predicting MMP is to combine experimental data and consider sensitive hydrocarbon components affecting MMP. Glaso (1985) presented a MMP correlation, which not only requires less CPU time but considers the sensitive factors such as reservoir temperature, the heavy components (C_{7+}) and intermediate components (C_2-C_6). If the international system of units is used in Glaso's correlation, then: see Equation (1), where *MMP*: Minimum Miscibility Pressure (MPa); $M_{C_7^+}$: molar weight of C_7^+; T_{RC}: reservoir temperature (°C); f_{RF}: mole fraction of components, C_2-C_6.

$$MMP = (2947.9 - 3.404 \times M_{C_7^+} + [1.700 \times 10^{-9} M_{C_7^+}^{3.73} \times e^{(786.3 M_{C_7^+}^{-1.058})}](1.8 T_{RC} + 32) - 121.2 f_{RF}) \times 0.006895 \quad (1)$$

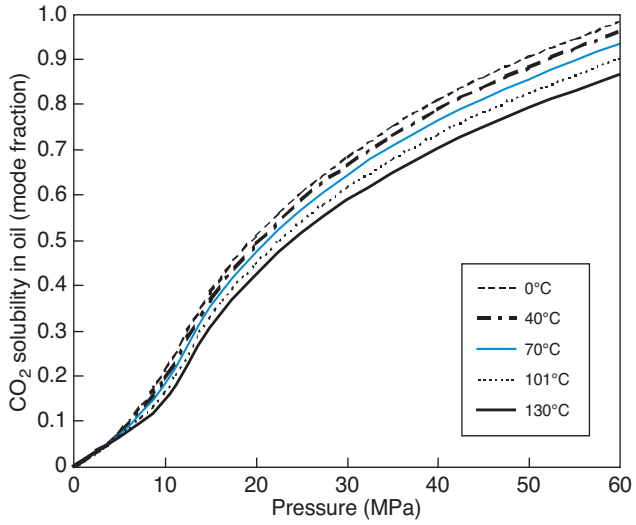

Figure 2

CO_2 equilibrium solubility in the crude oil (experimental data).

1.3.2 CO_2 Equilibrium Solubility in Oil

CO_2 equilibrium solubility in a crude oil depends on oil components, pressure and temperature. It is difficult to accurately calculate the solubility by using a correlation at any pressure and temperature. An experimental approach can provide CO_2 equilibrium solubility in a specific crude oil. In this work, the experimental solubility in the JL oil sample (CNPC, China) is shown in Figure 2. Interpolation approach is used to calculate the solubility in the oil at a specified pressure and temperature (P, T).

1.4 Governing Equations

The physical processes associated with CO_2, oil and water flow in porous media are governed by the laws such as conservation of mass, momentum and energy. These physical laws can be represented mathematically at the macroscopic level by a set of partial differential or integral equations. To derive a set of generalized governing equations for multiphase fluid flow, multicomponent transport and heat transfer, we assume that these processes can be described using a continuum approach within a Representative Elementary Volume (REV) in a porous medium. In addition, a condition of local thermodynamic equilibrium and partitioning is assumed so that temperatures, phase pressures, densities, viscosities, enthalpies, internal energies and component concentrations (or mole fractions) at any time are the same locally, respectively, at each REV of the porous medium.

1.4.1 Mass Conservation Equations

According to mass conservation principles, a conservation equation of mass components in a porous medium can be written as follows:

$$\frac{\partial A^k}{\partial t} = F^k + q^k \tag{2}$$

where superscript k is the index for the components, $k = 1, 2, 3, \ldots, N_c$, with N_c being the total number of mass components; A^k is the accumulation term of component k; q^k is an external source/sink term for mass component k; and F^k is the "flow" term of mass or diffusive and dispersive mass transport.

The accumulation terms in Equation (2) for component k is written as:

$$A^k = \phi \sum_{\beta} \left(\rho_\beta S_\beta X_\beta^k \right) + \rho_\beta \delta^k \quad (k = 1,\ 2,\ 3,\ \ldots,\ N_c) \tag{3}$$

where subscript β is an index for fluid phase (β = g for gas phase, = w for aqueous phase, = o for oil phase); ϕ is the porosity of porous media; ρ_β is the density of phase β; and S_β is the saturation of phase β; X_β^k is the mole fraction of component k in fluid β; δ^k is the volume of component k deposited on the pore surfaces per unit bulk volume. Its adsorption rate may be described as:

$$R_s^k = \frac{\partial \delta^k}{\partial t} = \alpha_d^k v_o X_\beta^k \quad (k = 1,\ 2,\ 3,\ \ldots,\ N_c) \tag{4}$$

where α_d^k is a capture rate coefficient of component k at pore walls. v_o is the flow velocity of oil phase. R_s^k is the adsorption rate of component k on rock solids. Some heavy components such as asphalt and asphaltene have more opportunity to attach on pore walls, which leads to formation damage.

The mass component transport is governed by processes of advection, diffusion and dispersion. Based on T2R3D code of the TOUGH2 family, the total mass flow term (Scheidegger, 1961; Wu and Pruess, 2000) for a component k is written as:

$$F^k = -\sum_{\beta} \nabla \bullet \left(\rho_\beta X_\beta^k \mathbf{v}_\beta \right) + \sum_{\beta} \nabla \bullet \left(\underline{D}_\beta^k \bullet \nabla \left(\rho_\beta X_\beta^k \right) \right) \quad (k = 1,\ 2,\ 3,\ \ldots,\ N_c) \tag{5}$$

where $\mathbf{v}_\beta$ is a vector of volumetric flow rate for fluid flow, defined by Darcy's law to describe the multiphase flow as:

$$\mathbf{v}_\beta = -\frac{k' k'_{r\beta}}{\mu_\beta} \left(\nabla P_\beta - \rho_\beta g \nabla z \right) \tag{6}$$

where, P_β, μ_β and g are pressure, viscosity of fluid phase β and gravitational constant, respectively; z is the vertical coordinate. k' is absolute permeability; and $k'_{r\beta}$ is the relative permeability to phase β. In Equation (5), $\underline{D}_\beta^k$ is the hydrodynamic dispersion tensor accounting for both molecular diffusion and mechanical dispersion for component k

in phase β, defined by an extended dispersion model (Scheidegger, 1961) to include multiphase effects (Wu and Pruess, 2000) as:

$$\underline{D}_\beta^k = \alpha_T^\beta \left|\mathbf{v}_\beta\right| \delta_{ij} + \left(\alpha_L^\beta - \alpha_T^\beta\right) \frac{\mathbf{v}_\beta \mathbf{v}_\beta}{\left|\mathbf{v}_\beta\right|} + \phi S_\beta \tau d_\beta^k \delta_{ij} \quad (k = 1,\ 2,\ 3,\ \ldots,\ N_c) \tag{7}$$

where α_T^β and α_L^β are transverse and longitudinal dispersivities, respectively, in fluid β; τ is the tortuosity of a porous medium; d_β^k is the molecular diffusion coefficient of component k within fluid β; and δ_{ij} is the Kronecker delta function ($\delta_{ij} = 1$ for $i = j$; and $\delta_{ij} = 0$ for $i \neq j$), with i and j being coordinated indices.

1.4.2 Energy Conservation Equations

Heat transfer in porous media is in general a result of both convective and conductive heat transfer processes, while radiation may be ignored in most cases. These processes are complicated by mass transfer between multiphase fluids, multicomponents, associated changes in phases, internal energy and enthalpy. The energy conservation equations in a porous medium system (rock) may be described as:

$$\frac{\partial}{\partial t}\left\{\sum_\beta \left(\phi\, \rho_\beta S_\beta U_\beta\right) + \left(1-\phi\right) \rho_s U_s\right\} - q^T = -\sum_\beta \nabla \bullet \left(h_\beta \rho_\beta \mathbf{v}_\beta\right) + \sum_\beta \sum_k \nabla \bullet \left(h_\beta^k \underline{\mathbf{D}}_\beta^k \bullet \nabla\left(\rho_\beta x_\beta^k\right)\right) + \nabla \bullet \left(K_T \nabla T\right) \tag{8}$$

where ρ_s is the density of rock grains; U_β and U_s are the internal energies of fluid β and rock grains, respectively. q^T is the external source/sink term for energy; h_β and h_β^k are the specific enthalpies of fluid phase β and of component k in fluid β, respectively; K_T is the overall thermal conductivity; and T is temperature.

1.4.3 Constitutive Relationships and Fluid Properties

To complete the mathematical description of multiphase flow, multicomponent transport and heat transfer in porous media, the mass and energy-balance equations need to be supplemented with a number of constitutive equations. These correlations express interrelationships and constraints of physical processes, variables and parameters and allow the evaluation of secondary variables and parameters as functions of a set of primary unknowns or variables selected to make the governing equations solvable. The constitutive correlations are expressed as the following.

Constraint on the summation of total fluid saturation in porous media satisfies as:

$$\sum_\beta S_\beta = 1 \tag{9}$$

Constraint on mole fractions within phase β is written as:

$$\sum_k X_\beta^k = 1 \tag{10}$$

In a multiphase system, the capillary pressure between two phases is defined as functions of fluid saturation:

$$P_{C\beta} = P_{C\beta}\left(S_\beta\right) \tag{11}$$

The relative permeability of a fluid phase in a two-phase system is normally assumed to be functions of its saturation:

$$k_{r\beta}^{'} = k_{r\beta}^{'}\left(S_\beta\right) \tag{12}$$

Although the relative permeabilities and capillary pressures functions can be described by previous correlations (Pruess *et al*., 1999), experimental work generally provides experimental data. In this work, relative permeabilities and capillary pressures are show in Figure 3.

The density of a fluid phase is treated as a function of pressure and temperature, as well as mole fraction (k = 1, 2, 3, ..., N_c):

$$\rho_\beta = \rho_\beta\left(P, T, X_\beta^k\right) \tag{13}$$

The density of each phase can be regarded as a function of pressure, temperature and compositions. For the aqueous phase, the effects of hydrocarbons dissolved in the phase on its density can be neglected. A modification of the model (Garcia, 2001; Pruess, 2005) is:

$$\rho_{aq} = \left(\frac{1 - X_w^{CO_2}}{\rho_w} + \frac{X_w^{CO_2}}{\rho_{CO_2}}\right)^{-1} \tag{14}$$

For gas phase, a version of the SRK equation with modified coefficients is used to gas density. The multicomponent versions of two parameters in SRK are written in terms of parameters a_k, b_k and gas phase mole fractions X_g^k of the individual components using the mixing rules recommended by Reid *et al*. (1987).

The density of CO_2-oil mixture calculated by PR or SRK equations is inaccurate. Based on PR equation, we developed a New State Equation (NSE) to calculate the density:

$$P = \frac{RT}{V - b_m} - \frac{(a\alpha)_m + \beta_m}{(V + b_m)^2 - c b_m^{\,2}} \tag{15}$$

where:

$$(a\alpha)_m = \left[\sum_{i=1}^n \sum_{j=1}^n x_i x_j \sqrt{a_i a_j \alpha_i \alpha_j}\right]^2 \tag{16}$$

$$\beta_m = \sum_{i=1}^n \left(601.68 x_i \frac{T}{T_{ci}} \omega_i\right)^{3.5} \tag{17}$$

$$a_m = \left(\sum_k X_g^k \sqrt{a_k}\right)^2 \tag{18}$$

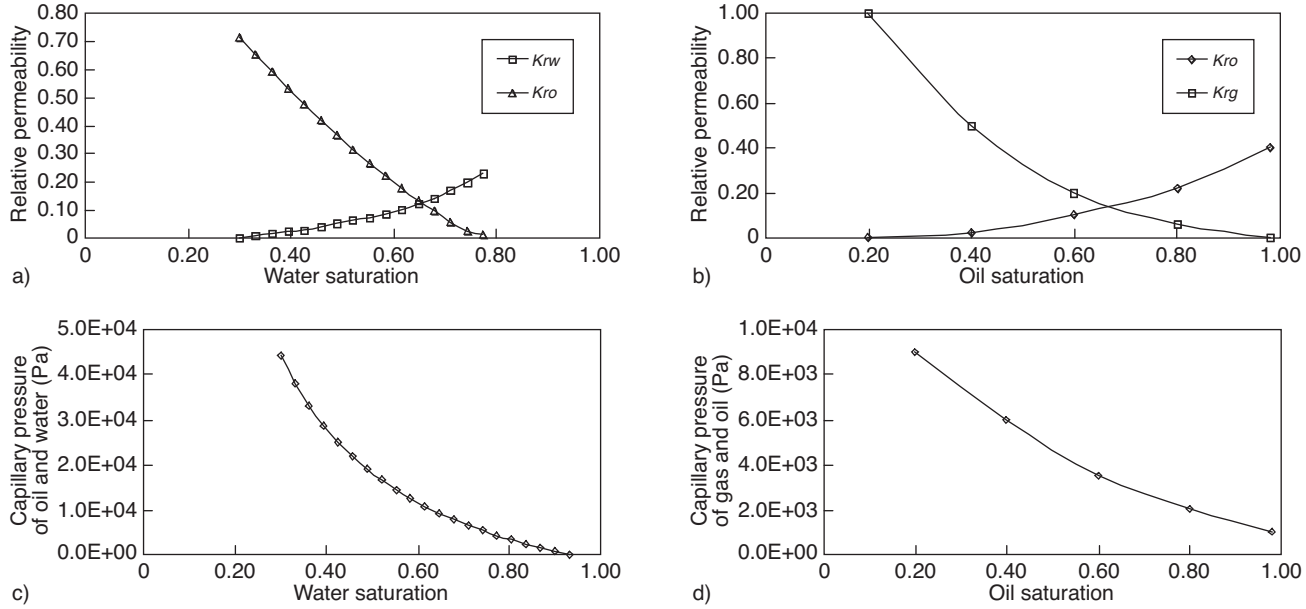

Figure 3

The relative permeabilities and capillary pressures. a) The relative permeability curve of oil and water; b) the relative permeability curve of gas and oil; c) the capillary pressure curve of oil and water; d) the capillary pressure curve of gas and oil.

$$b_m = \sum_k X_g^k b_k \tag{19}$$

Table 1 gives the densities of CO_2-oil mixture predicted by the equations (PR, SRK and NSE). The Comparison of experimental data and calculated results validates NSE.

The empirical expression of viscosity of a fluid is treated as a function of pressure, temperature and composition:

$$\mu_\beta = \mu_\beta \left(P, T, X_\beta^k\right) \tag{20}$$

The mixture viscosity of each phase is obtained in terms of the pure component viscosities as:

$$\mu_\beta = \sum_{k=1}^{N_c} X_\beta^k \mu_k \tag{21}$$

The viscosity of each component is calculated as a function of temperature from an equation due to Yaws *et al*. (1976):

$$\ln \mu_k = A' - \frac{B'}{T} + C'T + D'T^2 \tag{22}$$

Equilibrium partitioning X_α^h and X_β^h are the mole fraction of component k in phase α and β, respectively; and $K_{\alpha:\beta}^h$ is the equilibrium partitioning coefficient of component k between phases α and β. Their relation is:

$$X_\alpha^k = K_{\alpha:\beta}^k X_\beta^k \tag{23}$$

TABLE 1

Comparison of experimental data and calculated results (reservoir temperature is 108.4°C)

Pressure (MPa)	Density (kg/m^3)				Relative error (%)		
	Experimental data	SRK	PR	NSE	SRK	PR	NSE
35.00	759.00	612.26	714.40	758.16	19.33	7.28	0.12
33.00	757.20	610.26	713.56	756.99	19.41	7.15	0.03
31.00	755.40	608.16	712.69	755.76	19.21	6.86	0.22
29.00	753.60	605.94	711.79	754.48	19.30	6.73	0.30
27.00	751.80	603.58	710.86	753.15	19.40	6.60	0.38
25.00	749.90	601.08	709.91	751.76	19.51	6.47	0.46
23.00	748.10	598.41	708.91	750.29	19.65	6.35	0.52
21.26	746.40	595.94	708.02	748.96	19.83	6.26	0.55
19.00	744.20	592.51	706.82	747.12	19.92	6.07	0.67
17.00	742.30	589.23	705.71	745.39	20.18	5.99	0.68
15.00	740.30	585.69	704.56	743.53	20.41	5.87	0.72
13.00	738.30	581.84	703.37	741.53	20.67	5.76	0.74
11.00	736.30	577.65	702.13	739.34	21.55	5.92	0.43
10.41	735.70	576.33	701.75	738.65	21.66	5.89	0.42

Partitioning coefficient depends on chemical properties of the component and is a function of temperature, pressure and composition:

$$K_{\alpha:\beta}^{k} = K_{\alpha:\beta}^{k}\left(P_{\beta}, T, X_{\beta}^{k}\right) \tag{24}$$

Considering the choice of primary variables, we treat oil as reference phase in this work. The details of calculating equilibrium partitioning coefficient are discussed by Ahmed (2007).

Specific enthalpy of a liquid is expressed as:

$$h_{\beta} = U_{\beta} + \frac{P_{\beta}}{\rho_{\beta}} \tag{25}$$

Internal energy, U_{β}, of liquid phase β is a function of composition, pressure and temperature. Specific enthalpy of a gas is expressed as:

$$h_{g}^{k} = U_{g}^{k} + \frac{P_{g}^{k}}{C_{g}^{k}} \tag{26}$$

U_{g}^{k} is the specific internal energy of component k in the gas phase; C_{g}^{k} is the partial density of component k in gas phase.

The thermal conductivity of a porous medium is treated as a function of fluid saturation:

$$K_{CT} = K_{CT}\left(S_{\beta}\right) \tag{27}$$

Porosity, ϕ^{0}, is the effective porosity at a reference pressure, P_0 and a reference temperature, T_0; and C_r and C_T are the compressibility and thermal expansion coefficient of the medium, respectively:

$$\phi = \phi^{0}\left[1 + C_{r}(P - P_{0}) - C_{T}(T - T_{0})\right] \tag{28}$$

The adsorption of heavy components on pore surfaces may lead to the reduction in a local porosity and permeability of the medium. The instantaneous porosity is expressed by:

$$\phi' = (\phi - \Delta\phi) \tag{29}$$

where $\Delta\phi$ denotes the variation of the porosity caused by an adsorption of heavy components on pore walls and it is expressed by:

$$\Delta\phi = \sum \delta^{k} \tag{30}$$

δ^{k} can be calculated by the integration of Equation (4). That is:

$$\delta^{k} = \int_{0}^{t} \alpha_{d}^{k} v_{o} X_{\beta}^{k} \tag{31}$$

To describe mathematically the formation damage caused by asphaltene precipitation, the heaviest pseudo-oil component (k = asphaltene) is approximately treated as asphaltene. δ^{k} is generally equal to zero at initial time. The theory of asphaltene precipitation and deposition and its mathematical modeling was discussed in details by Ju *et al*. (2010). The change in permeability addressed in this study is caused by asphaltene. According to the reference (Liu and Faruk, 1993), the expression for instantaneous permeability changed by asphaltene precipitation is given by:

$$k' = k_{0}'[(1 - f)\lambda_{f} + f\phi / \phi_{0}]^{n} \tag{32}$$

in which k_{0}' and ϕ_0 are the initial permeability and porosity; k' and ϕ are instantaneous local permeability and porosity of a porous medium; and λ_f is a constant for fluid seepage allowed by the plugged pores. The range of index n is from 2.5 to 3.5. f is a flow efficiency factor (Ju *et al*., 2002).

2 NUMERICAL SOLUTION SCHEME

The total number of mass components and energy equation is $N_c + 1$. There is a total of N_c mass conservation equations to solve for an isothermal reservoir; and $N_c + 1$ equations to solve for a non-isothermal system. The selections of primary variables are listed in Table 2.

In Table 2, phase g denotes CO_2 phase of gaseous, supercritical, or liquid state; m is phase index for oil- CO_2 mixture; and X_{m}^{h} is a mole fraction of component k in oil-CO_2 mixture phase.

In this work, the integral finite-difference method is used for spatial discretization. Time discretization is carried out using a backward, first-order, fully implicit finite-difference scheme. The details of the discretization and numerical solution procedure are discussed in the TOUGH2 literature (Pruess *et al*., 1999).

TABLE 2

Primary variables and their switching scheme due to changes in phase condition

Phase condition	Phase index	Primary variables							
		1	2	3	4	…	N_c–1	N_c	N_c+1
Two-phase: water and oil ($P \le$ MMP, immiscible)	Scenario-1	P_o	X_o^3	X_o^4	X_o^5	…	$X_o^{N_c}$	S_w	T
Three-phase: water, oil and CO_2 (gas) ($P \le$ MMP, immiscible)	Scenario-2	P_o	S_g	X_o^4	X_o^5	…	$X_o^{N_c}$	S_w	T
Two-phase: water and oil-CO_2 mixture ($P >$ MMP, miscible)	Scenario-3	P_m	X_m^3	X_m^4	X_m^5	…	$X_m^{N_c}$	S_w	T

3 NUMERICAL RESULTS AND DISCUSSIONS

This section demonstrates the functions of the developed simulator and validates the mathematical model describing the multiphase and multicomponent flow involving CO_2 displacement in oil formations. Although the model developed in this work can predict water solubility in oil phase, we neglect this effect because of very low solubility of water in the oil phase. In addition, CO_2 dissolving in the aqueous phase is also neglected for its slight effects on water properties.

3.1 The Comparison between Simulation and Slim Tube Data

In this section, the isothermal simulation result of one-dimensional miscible flooding is compared with the experimental data. The main parameters used in the numerical simulation are shown in Table 3. The MMP of the CO_2-oil system is 27.45 MPa, which is obtained by slim tube experiments. The crude oil used for the slim tube and CO_2 flooding experiments sampled from H75-27-7 well, H.G. Oil field, CNPC. Its viscosity and density at the reservoir condition are 1.86 mPa.s and 0.7542 g/cm^3. The initial pressure of each grid element and flow pressure at the outlet (the 10th element) is set at 32.27 MPa and 32.26 MPa, respectively, which results in miscible flooding during the flooding. The conditions such as pressure and temperature are the same in the numerical runs and experiments. The model grids and locations of the CO_2 injection and production sink are demonstrated in Figure 4.

TABLE 3

Main parameters of one-dimensional miscible flooding simulation

Parameter name	Value	Parameter name	Value
The node numbers	10	Connate water saturation	0.20
The size of grid elements along x (m)	1.00	Initial gas saturation	0.00
Initial temperature (°C)	101.60	Porosity	0.30
Initial pressure (MPa)	32.27	Permeability at x direction (10^{-3} μm^2)	160.00
Number of components in the oil mixture	5	CO_2 injection rate of each injection well (kg/s)	0.0001
Initial oil saturation	0.80	Wellbole flow pressures (MPa)	32.26

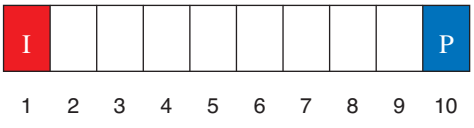

Figure 4

Model grid of CO_2 flooding for the numerical simulation example. I: CO_2 injection; P: oil production sink.

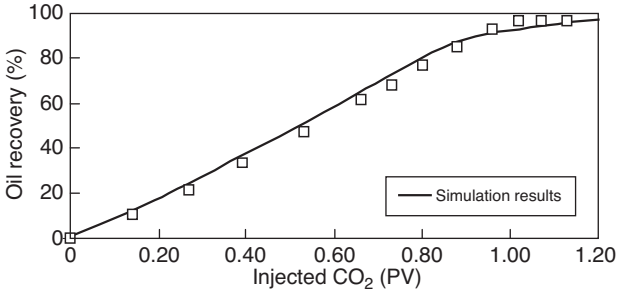

Figure 5

The comparison between the numerical results and experimental data (PV: pore volume at experimental pressure and temperature).

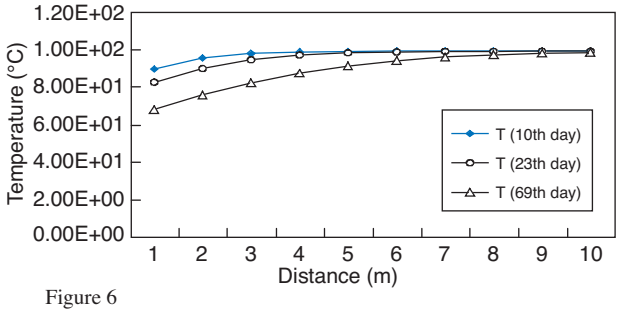

Figure 6

The temperature distribution of 1D simulation.

Figure 5 shows that the relation between the oil recovery and injection PV of CO_2 is almost linear before CO_2 breakthrough (0.88 PV at horizontal axis) at the outlet of the model. After CO_2 breakthrough, the improvement in oil recovery slows down with continuous injection. It also shows that the oil recovery obtained by numerical simulation has a good match with experimental data. Only small errors (maximum relative error is less than 2%) between the predicted results and experimental data. The oil recovery after 1.2 PV injection of CO_2 is also very closed to the result of Dong *et al*. (2001). The comparison with our experimental data and the published work (Dong *et al*., 2001) validates the reliability of the mathematical model in case of a miscible displacement. The high percentage of oil recovery at the miscible flooding indicates that the flooding in the 1D model can be regarded as piston-like displacement.

To demonstrate the temperature change during flow in 1D simulation, the temperature distribution of a non-isothermal numerical run is shown in Figure 6. The injection temperature of CO_2 is 51.2°C. The temperatures of the elements closed to the injection grid element (the first grid shown in *Fig. 4*) become much lower than that of other elements. The number of the elements with the temperatures lower than original temperatures (99°C) increases with the elapsed time of CO_2 injection. The temperatures of all elements become lower than original temperature at the 69th day.

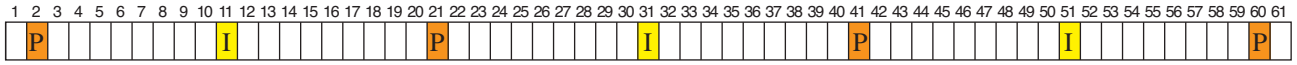

Figure 7

Model grid of CO_2 flooding for one dimensional simulation example. I: CO_2 injection source; P: oil production sink; the bulk of each block is 1 m^3.

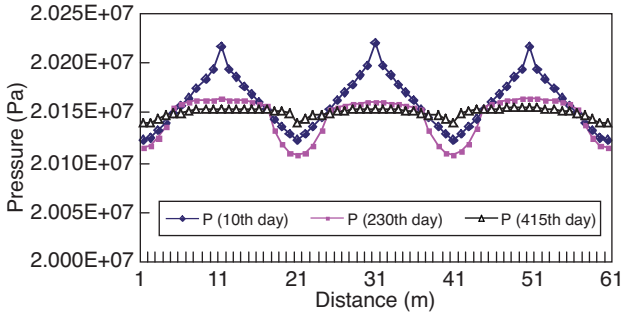

Figure 8

The oil phase pressure distribution at different injection time.

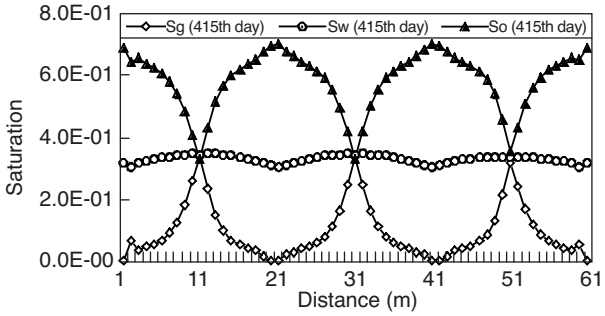

Figure 9

The saturations of oil, water and gas at the 415th day.

TABLE 4

Main parameters of one-dimensional immiscible flooding simulation

Parameter name	Value	Parameter name	Value
The node numbers	61	Initial water saturation	0.55
The size of grid elements along x (m)	1.00	Initial gas saturation	0.00
Initial reservoir temperature (°C)	99.000	Porosity	0.30
Initial reservoir pressure (MPa)	21.25	Permeability (10^{-3} μm^2)	16.00
Number of components in the oil mixture	5	CO_2 injection rate of each injection well (kg/s)	2.0E-5
Initial oil saturation	0.45	Wellbole flow pressures for all production wells (MPa)	20.14

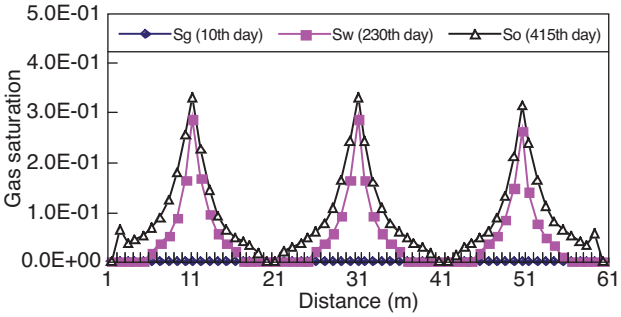

Figure 10

Gas saturations at the different time.

3.2 One Dimensional Immiscible Flooding Sample

The sample is a numerical test with a homogeneous geological model. Three sources of CO_2 at a same rate and four production sinks at a same specified wellbore flow pressure are considered *(Tab. 4)*. The geological model and the locations of these sources and sinks are shown in Figure 7. The distance between injection sources and production sinks is constant.

The oil-phase pressures along the one-dimensional model at the 10th, 230th and 415th day are shown in Figure 8. The pressure reaches a maximum value at each injection element (a source location) and it reaches a minimum value at each production element (a sink location). It indicates that the pressure gradients between the injection and production grids reduce with the extension of injection time. The reduction in the pressure gradients may be explained as the decrease in flow resistance, which is caused by the decline of the viscosity of the oil-CO_2 mixture for more CO_2 dissolved in oil.

Figure 9 shows the saturations of three phases along the one-dimensional model after 415 days of CO_2 injection. At the locations (Element 11, 31 and 51) of CO_2 injection, gas saturations reach a maximum value and oil saturations reach a minimum value due to CO_2 injection into these grids at an immiscible condition. The symmetrical distributions of the three phases predicted by the simulator validate the stability of the numerical solution in view of symmetrical check for numerical iteration. Figure 10 shows the gas saturation distributions at three different times. At the 10th day, gas saturation in each grid is zero as the injected CO_2 is completely

dissolved into the oil phase. Gas (the mixture of CO_2 and light hydrocarbons such as methane, ethane) doesn't form from oil phase until the equilibrium solubility of CO_2 in oil is reached. Continuous CO_2 injection leads to CO_2 and light hydrocarbon's formation from oil and the increase in the numbers of the grids containing free gas. The gas phase almost exists in all grids at the 415th day.

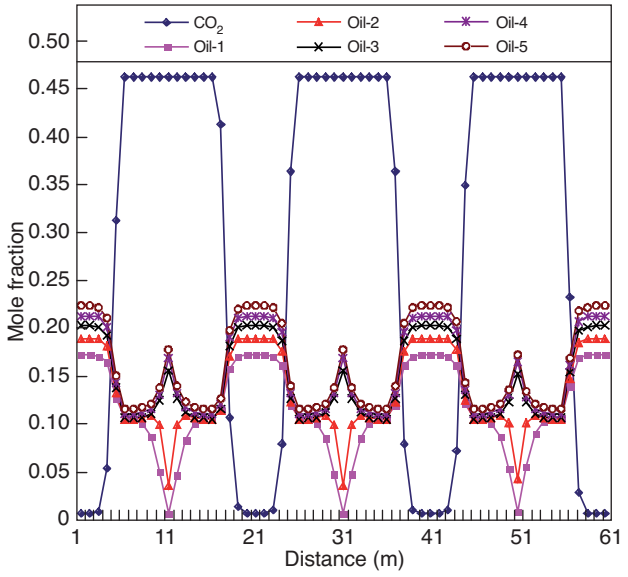

Figure 11

Mole fraction distribution in crude oil at the 132nd day.

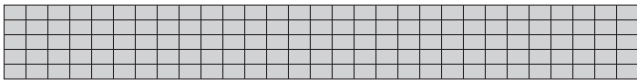

Figure 12

Model grid for the two-dimensional vertical section model.

Figure 11 shows the mole fraction of each component in oil phase in each grid at the 132nd day. In the simulation, the hydrocarbons in the crude are grouped into five pseudo-components (Oil-1, ..., Oil-5). It is assumed that CO_2 dissolves in oil, and water does not dissolve in oil. In the vicinity of the injection elements, CO_2 mole fraction reaches about 0.46 and it does not continuously rise even if more CO_2 injected. The reason is that the maximum mole solubility of CO_2 in the oil at the immiscible conditions is 0.46 and successive CO_2 injected in those grids will form free gas phase.

3.3 Two Dimensional Vertical Profile Flooding Sample

In this example, the CO_2 flooding performance in a two-dimensional cross sectional model is simulated. The generated grid:

$$N_x \times N_y \times N_z = 30 \times 1 \times 5 \text{ blocks} \tag{33}$$

is shown in Figure 12. The thickness of the model is 40 m, and its length is 300 m. The horizontal and vertical permeability are 0.16×10^{-12} m^2 and 0.02×10^{-12} m^2 respectively. The initial pressure is 20.18 MPa, and the other parameters are listed in Table 4. Figure 13 shows the CO_2 flooding profile at the 500th day. Three zones (regions) are shown in the profiles. Miscible zone locates in the upper region close to the perforated interval. In this zone, no gas phase exists due to the pressure greater than MMP. In immiscible zone, CO_2 does not completely dissolve in the oil. Oil-CO_2 mixture, water and gas phases coexist. In the unswept zone ahead of the immiscible region, only water and oil phases coexist. It implies that the spatial distribution of the three zones and flow characteristics is affected by gravitational difference between two phases. The sample demonstrates that the simulator is capable of simultaneously simulating miscible and immiscible flooding in different regions of an oil reservoir. Phase transfer will carry out automatically at the flooding front.

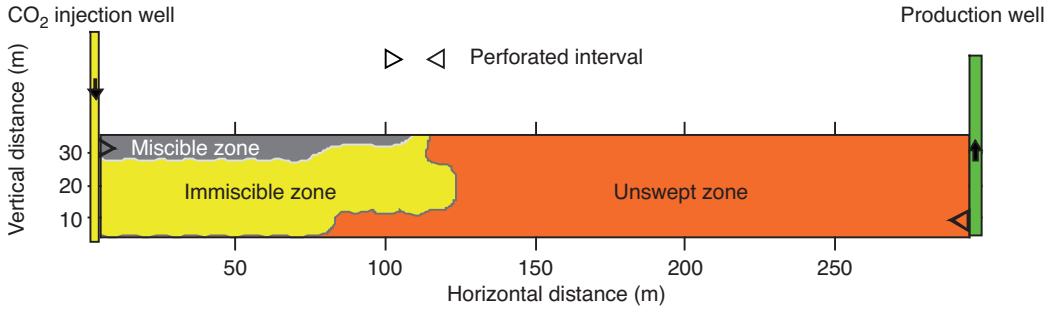

Figure 13

The CO_2 flooding profile at the 500th day since CO_2 injection.

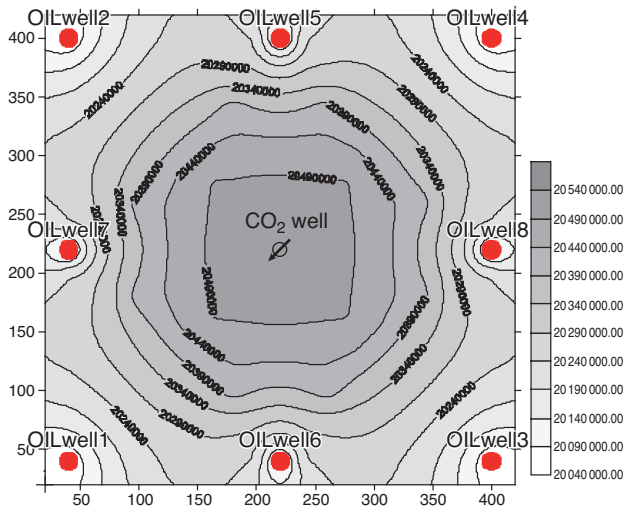

Figure 14

Pressure distribution at the 400th day since CO_2 injection.

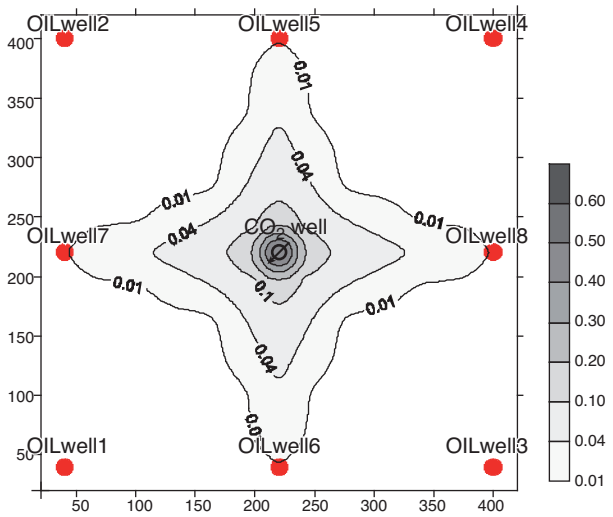

Figure 15

Gas saturation distribution at the 400th day after CO_2 injection.

TABLE 5

Main parameters of two-dimensional horizontal flooding simulation

Parameter name	Value	Parameter name	Value
The node numbers	441	Initial oil saturation	0.45
The size of grid elements along *x* (m)	20.00	Initial water saturation	0.55
The size of grid elements along *y* (m)	20.00	Initial gas saturation	0.00
The size of grid elements along *z* (m)	10.00	Porosity	0.30
Initial reservoir temperature (°C)	99.000	Permeability (10^{-3} μm^2)	90.00
Initial reservoir pressure (MPa)	20.179	CO_2 injection rate of each injection well (kg/s)	5E-2
Number of components in the oil mixture	5	Wellbore flow pressures for all production wells (MPa)	20.04

3.4 Two Dimensional Horizontal Flooding Sample

In this example, a simulation with nine wells has been performed to study the CO_2 immiscible flooding performances and the effects of asphaltene precipitation on formation damages. The main parameters for this example are shown in Table 5. A CO_2 injection well is located in the center of the square domain. Four production wells are located at four corners and the other four production wells are located at the mid-point of the four outer boundaries. All grids in the *x*-*y* plane are squares with same size. The wellbore flow pressure of each production well is assumed constant during the simulation.

Figure 14 gives the pressure contours of oil phase in oil formation. The symmetrical distribution of the pressure predicted by the simulator in the plane accords with the theoretical pressure distribution. It indicates that the pressure gradients near the injection well are much less than that of the production wells. The characteristics of pressure gradients imply that the flow resistance of the region near the source (injection well) is much lower than that of the sink locations. The production wells will benefit from the reduction in the flow resistance induced by CO_2 flooding.

The contours of gas saturation are shown in Figure 15. Gas breakthrough occurs at the edge wells (OILwell5 to OILwell8) on the 400th day since CO_2 injection. It is estimated that the area swept by injected CO_2 accounts for less than a half area of the domain after the gas breakthrough at the edge wells. This viscous fingering phenomenon prevents the expansion of CO_2 swept area, which is unfavorable for further EOR in view of corner production wells (OILwell1 to OILwell4). In addition, rectangular grids might sharpen the displacement fronts along the grid orientations (*x* or *y* direction), which might also affect the displacement performances. These effects could be reduced by using a nine or seven-point finite difference discretization scheme (Yanosik and McCracken, 1979; Pruess and Bodvarsson, 1983). Hybrid or polygonal grids also could be used to reduce the grid orientation effects.

Figure 16 shows the contours of the CO_2 mole fraction in oil phase after 400 days of CO_2 injection. The CO_2 swept area can be divided into two regions by the dot line (0.46 CO_2 mole fractions). The inner region, (the close region surrounded by the dot line) is saturated by water, oil and CO_2 rich gas. In addition, part of CO_2 dissolves in oil phase. The outer region of the dot line swept by CO_2 is saturated by water and oil

phases. Although the oil containing CO_2 in this region, the CO_2 mole fraction in oil is less than the equilibrium solubility. Therefore, no free gas phase exists in the region.

Asphaltene will start to flocculate from oil phase when the mole fraction of CO_2 in oil increases high enough. It may build up on pore walls or at pore throats of oil formation, leading to formation damage. The term permeability change is introduced to evaluate formation damage caused by asphaltene precipitation. It is defined as:

$$C_{perm} = \frac{k'}{k_0'} \times 100\% \tag{34}$$

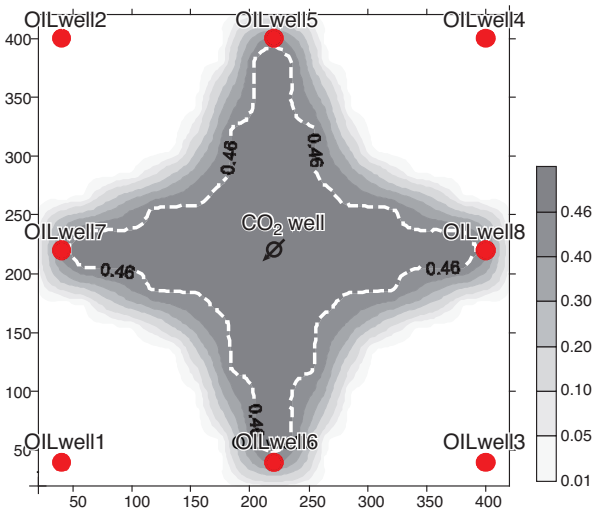

Figure 16

CO_2 mole fraction in oil at the 400th day after CO_2 injection.

Figure 17 shows that the formation damage region expands for the increase in sweep area by injected CO_2. However, the permeabilities in the location closed to CO_2 injection well are higher than that of the region away from the injection well. One reason is that the high-flow velocity in the region around the well may flush away part of the asphaltene adsorbed on pore surfaces, which leads to a reduction in the capture rates of asphaltene at the sites. The other reason is that the pores in the region closed to injection well is almost saturated by CO_2. Therefore, only a small amount of solid asphaltene formed because of low oil saturation in the pores of the region.

CONCLUSION

This study was performed to develop a non-isothermal compositional mathematical model for predicting CO_2 miscible and immiscible flooding performances in oil reservoirs for EOR. Physical and chemical processes such as heat transfer, convection-diffusion-adsorption, porosity and permeability changes induced by asphaltene deposition are fully considered during CO_2 flow in porous media. Three scenarios of fluid phases and phase transfer are implemented by checking the MMP and CO_2 equilibrium solubility after the updates of primary variables. Automatic switches of the variables are assigned for the numerical solution according to corresponding phase scenarios.

The governing equations for CO_2 flooding were discretized in space using the integral implicit finite-difference method developed for the TOUGH2 family of reservoir simulators. Newton-Raphson iterative technique was used to solve the nonlinear equation system and a numerical reservoir simulator

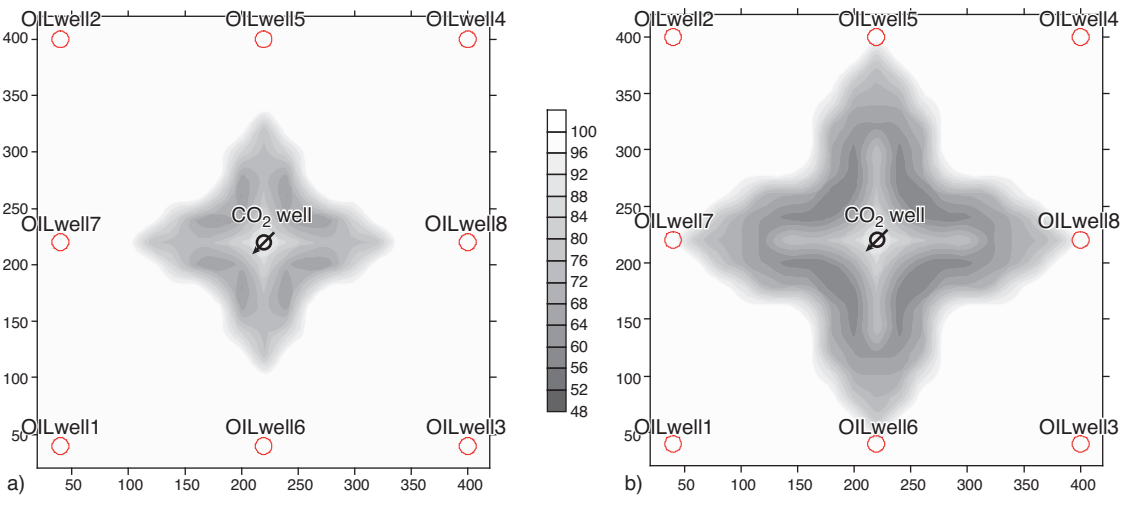

Figure 17

The distribution of permeability change caused by asphaltene precipitation. a) At the 150th day after CO_2 injection; b) at the 400th day after CO_2 injection.

was developed in FORTRAN code based on the T2R3D simulator belonging to the TOUGH2 family of computer codes.

Four examples demonstrate the various functions of the simulator developed in this work. The comparison of one-dimensional miscible simulation results with the experimental data validates the reliability of the mathematical model and the simulator. Symmetrical distributions of the predicted parameters such as pressure, saturations and mole fraction in the second and fourth examples imply that the numerical solution passes the symmetrical test. The displacement front and the interface between miscible and immiscible zones can be traced during the simulation of the third sample. The distributions of temperature and permeability change caused by temperature-independent asphaltene precipitation were also analyzed in the first and fourth examples.

The four examples not only imply that the simulator developed for CO_2 flooding for EOR is robust but also demonstrate the functional variety of phase scenarios. However, further research should focus on a precise correlation (a function of pressure, temperature and components) for predicting CO_2 solubility in oil phases and the effects of geological heterogeneity and grid orientations on flooding performances in actual oil reservoirs.

ACKNOWLEDGMENTS

This work was co-sponsored by SRF for ROCS, SEM, the national science and technology major projects 2011ZX05009-002/2011ZX05009–006, the Fundamental Research Funds for the Central Universities (CUGB), and the joint research on "Investigation of Mathematical Models and Their Applications for Oil, Water and CO_2 Flow in Reservoirs" between Colorado School of Mines, USA and Research Institute of Petroleum Exploration & Development, CNPC, of which are high appreciated. The authors would like to thank all anonymous reviewers and the Editorial Board members for their insightful and constructive comments and suggestions for improving the manuscript.

REFERENCE

Ahmed T. (2007) *Equations of State and PVT Analysis*, Gulf Publishing Company, Houston.

Bielinski A. (2007) Numerical Simulation of CO_2 Sequestration in Geological Formations, *PhD Thesis*, Stuttgart University.

Battistelli A., Marcolini M. (2009) TMGAS: a new TOUGH2 EOS module for the numerical simulation of gas mixtures injection in geological structures, *Int. J. Greenhouse Gas Control* **3**, 4, 481-493.

Garcia J.E. (2001) *Density of aqueous solutions of CO_2*, Lawrence Berkeley National Laboratory. http://escholarship.org/uc/item/6dn022hb.

Dong M.Z., Huanga S., Dyerb S.B., Mourits F.M. (2001) A comparison of CO_2 minimum miscibility pressure determinations for Weyburn crude oil, *J. Petrol. Sci. Eng.* **31**, 1, 13-22.

Glaso O. (1985) Generalized Minimum Miscibility Pressure Correlation, *SPE J.* **25**, 6, 927-934.

Jaramillo P., Griffin W.M., McCoy S.T. (2009) Life cycle inventory of CO_2 in an enhanced oil recovery system, *Environ. Sci. Technol.* **43**, 21, 8027-8032.

Ju B.S., Dai S., Luan Z., Zhu T. (2002) A Study of Wettability and Permeability Change Caused by Adsorption of Nanometer Structured Polysilicon on the Surface of Porous Media, *SPE Asia Pacific Oil and Gas Conference and Exhibition*, Melbourne, Australia, 8-10 Oct.

Ju B.S., Qiu X.F., Qin J.S., Chen X.L., Fan T.L. (2010) Asphaltene Deposition and its Effects on Production Performances in the Development of Oil Field by CO_2 Flooding: a Numerical Simulation Assessment, *SPE EUROPEC/EAGE Annual Conference and Exhibition*, Barcelona, Spain, 14-17 June.

Lal R. (2008) Sequestration of atmospheric CO_2 in global carbon pools, *Energ. Environ. Sci.* **1**, 86-100.

Lichtner P.C. (2003) FLOTRAN user's manual: two-phase non-isothermal coupled thermal-hydrologic chemical (THC) reactive flow and transport code, Los Alamos National Laboratory, Report LA-UR-01-2349.

Liu X., Faruk C. (1993) Characterization and Prediction of Formation Damage in Two-Phase Flow Systems, *the Production Operations Symposium*, Oklahoma City, OK, USA, 21-23 March.

Nghiem L., Sammon P., Grabenstetter J., Ohkuma H. (2004). Modeling CO_2 Storage in Aquifers with a Fully-Coupled Geochemical EOS Compositional Simulator, *SPE/DOE Symposium on Improved Oil Recovery*, *SPE* 89474, Tulsa, Oklahoma, 17-21 April.

Nitao J.J. (1998) *Reference Manual for the NUFT flow and transport code*, Version 2.0, Lawrence Livermore National Laboratory, and UCRL-MA-130651.

Petrusak R., Riestenberg D., Goad P. (2009) World Class CO_2 Sequestration Potential in Saline Formations, Oil and Gas Fields, Coal, and Shale: the US Southeast Regional Carbon Sequestration Partnership Has It All, *2009 SPE International Conference on CO_2 Capture, Storage, and Utilization*, San Diego, California, USA, 2-4 Nov.

Pinczewski V., Stevenson M. (2007) *SIMED II*, CSISO and School of Petroleum Engineering, University of New South Wales.

Pruess K., Bodvarsson G.S. (1983) A seven-point finite difference method for improved grid orientation performance in pattern steamfloods, *SPE* 12252, *Reservoir Simulation Symposium, 1983*, San Francisco, CA, USA, 15-18 Nov.

Pruess K. (2005) TOUGH2 Fluid Property Module for Mixtures of Water, NaCl, and CO_2, *Technical Report*, LBNL-57952, Lawrence Berkeley National Laboratory.

Pruess K. (2011) ECO2M: A TOUGH2 Fluid Property Module for Mixtures of Water, NaCl, and CO_2, Including Super- and Sub-Critical Conditions, and Phase Change Between Liquid and Gaseous CO_2, *LBNL Paper* LBNL-4590E.

Pruess K., Oldenburg C., Moridis G. (1999) *TOUGH2 User's Guide*, Version 2.0, Lawrence Berkeley National Laboratory, Berkeley, California, Report LBNL-43134.

Rackley S.A. (2010) *Carbon Capture and Storage*, USA Elsevier Inc, Burlington.

Rashid S.H.A.M., Sultan Q.U. (2003) Asphaltene Precipitation and Alteration of Wetting: The Potential for Wettability Changes During Oil Production, *SPE Reserv. Evalu. Eng.* **6**, 4, 210-214.

Reid R.C., Prausnitz J.M., Poling B.E. (1987) *The Properties of Gases and Liquids*, McGraw-Hill, New York.

Sams W.N., Bromhal G., Odusote O., Jikich S., Ertekin T., Smith D.H. (2002) Simulating Carbon Dioxide Sequestration/ECBM Production in Coal Seams: Effects of Coal Properties and Operational Parameters, *2002 SPE Eastern Regional Meeting*, Lexington, KY, 23-25 Oct.

Scheidegger A.E. (1961) General theory of dispersion in porous media, *J. Geophys. Res.* **66**, 10, 3273-3278.

Shedid A., Zekri Abdulrazag Y. (2006) Formation Damage Caused by Simultaneous Sulfur and Asphaltene Deposition, *SPE Prod. Oper.* **21**, 1, 58-64.

Shtepani E. (2006) Hycal Energy Research Laboratories Ltd. CO_2 Sequestration in Depleted Gas/Condensate Reservoirs, *2006 SPE Annual Technical Conference and Exhibition*, San Antonio, Texas, USA, 24-27 Sept.

Thawer R., Nicoll D.C.A., Graeme D. (1990) Asphaltene Deposition in Production Facilities, *SPE Prod. Eng.* **5**, 4, 475-480.

White M.D. (2003) *STOMP Subsurface Transport Over Multiple Phases: Users's Guide*, Version 2.0 Pacific Northwest National Laboratory, PNNL-14286.

Wu Y.S., Pruess K. (2000) Numerical simulation of non-isothermal multiphase tracer transport in heterogeneous fractured porous media, *Adv. Water Resour.* **23**, 7, 699-723.

Yanosik J.L., McCracken T.A. (1979) A Nine-Point, Finite-Difference Reservoir Simulator for Realistic Prediction of Adverse Mobility Ratio Displacements, *SPE* 5734, *SPE J.* **19**, 4, 253-261.

Yaws C.L., Miller J.W., Shah P.N., Schorr G.R., Patel P.M. (1976) Correlation Constants for Chemical Compounds, *Chem. Eng. Sci.* **83**, 24, 153-162.

Zheng Z., Larson E.D., Li Z., Liu G., Williams R.H. (2010) Near-term mega-scale CO_2 capture and storage demonstration opportunities in China, *Energ. Environ. Sci.* **3**, 9, 1153-1169.

Final manuscript received in February 2012
Published online in May 2013

Cite this article as: B. Ju, Y. Wu and J. Qin (2013). Computer Modeling of the Displacement Behavior of Carbon Dioxide in Undersaturated Oil Reservoirs, *Oil Gas Sci. Technol* **70**, 6, 951-965.